ADVANCED FUNCTIONAL MATERIALS
www.afm-journal.de

Polymorphic Kondo Effects Driven by Spin Lattice Coupling in VTe_2

Dongyeun Won, Do Hoon Kiem, Woohyun Cho, Sang-Hyeok Yang, Young-Hoon Kim, Young-Min Kim, Suyeon Cho, Myung Joon Han,* and Heejun Yang**

Polymorphism in transition metal dichalcogenides (TMDs) allows unique physical properties to be controlled, such as artificial heavy fermion phenomena, the quantum spin Hall effect, and optimized device operations with 2D materials. Besides lattice structural and metal-semiconductor polymorphs, intriguing charge density wave (CDW) states with different electronic and magnetic phases are demonstrated in TMDs. Typically, the "normal" state is stabilized at high temperature above the CDW energy scale, and therefore, is not relevant to many low-temperature quantum phenomena, such as magnetic ordering and the heavy fermion Kondo state. Here, a local and robust phase manipulation of the normal (1T) and CDW (1T') states of VTe_2 is reported by laser irradiation, and polymorphic Kondo effects are demonstrated with the two phases at low temperatures. The theoretical calculations show that Kondo screening of vanadium 3d electron moments is markedly enhanced in 1T'-VTe_2, which is responsible for the observed transport properties distinct from its 1T counterpart. Controlling the spin-lattice coupling and Kondo physics via laser-driven CDW phase patterning allows the design of correlated electronic and magnetic properties in TMDs.

1. Introduction

Phase engineering of transition metal dichalcogenides (TMDs) has been used to investigate critical quantum states,[1,2] including superconductivity,[3] 2D magnetism,[4] charge density wave (CDW),[5] and the metal-insulator transition (MIT).[6–8] Most quantum states in TMDs are manipulated by tuning temperature,[8,9] carrier density,[10,11] or pressure.[12] For certain TMDs, the energy differences between their structural and quantum phases (polymorphs) are small, which allows the coexistence of multiple phases in ambient conditions, known as TMD polymorphism. As a result, critical breakthroughs can be achieved for electronic devices with 2D materials, based on polymorphs with metallic and semiconducting states.[13] For example, homojunction devices with 2D MoS_2 and $MoTe_2$ have demonstrated optimized performances with low contact resistance and high carrier mobility.[6,14,15] Despite the practical use of metallic and semiconducting polymorphs of TMDs, some exotic quantum states (e.g., magnetic ordering or Kondo effects) of numerous high-temperature phases of TMDs have not been explored; investigating such states requires low-temperature measurements that are not accessible with the high temperature ('normal') phases of TMDs.

Vanadium ditelluride (VTe_2) is a magnetic 2D material with multiple CDW states.[4,16–19] Although its room temperature CDW phase (hereafter referred to as 1T'-VTe_2)[20,21] is distinct from 1T-VTe_2, the normal counterpart above T = 480 K,[4] recent studies have reported that atomically thin VTe_2 on certain substrates[22–26] and bulk VTe_2 samples grown by the molten-salt method[27] can have a normal 1T structure at room temperature. The coexistence of the normal and CDW states in ambient conditions demonstrates there is a small energy difference between the normal (1T) and CDW (1T') states of VTe_2, as similarly reported for the 2H and 1T' phases of $MoTe_2$. The unique polymorphism in this correlated quantum material, VTe_2, provides an exciting platform to investigate exotic magnetic phenomena such as the Kondo effect[28] based on clear crystallographic information and phase patterning technique.

Laser irradiation has become a practical method for phase engineering.[6] The two basic functions of laser irradiation are "local excitation of electrons in the material" and "local heating". Other effects such as oxidation and/or thinning have been carefully avoided in phase engineering

D. Won, S.-H. Yang, Y.-H. Kim, Y.-M. Kim
Department of Energy Science
Sungkyunkwan University
Suwon 16419, South Korea
D. H. Kiem, W. Cho, M. J. Han, H. Yang
Department of Physics
Korea Advanced Institute of Science and Technology (KAIST)
Daejeon 34141, South Korea
E-mail: mj.han@kaist.ac.kr; h.yang@kaist.ac.kr
S. Cho
Division of Chemical Engineering and Materials Science
Graduate Program in System Health Science and Engineering
Ewha Womans University
Seoul 03760, South Korea
E-mail: s.cho@ewha.ac.kr

The ORCID identification number(s) for the author(s) of this article can be found under https://doi.org/10.1002/adfm.202313180

DOI: 10.1002/adfm.202313180

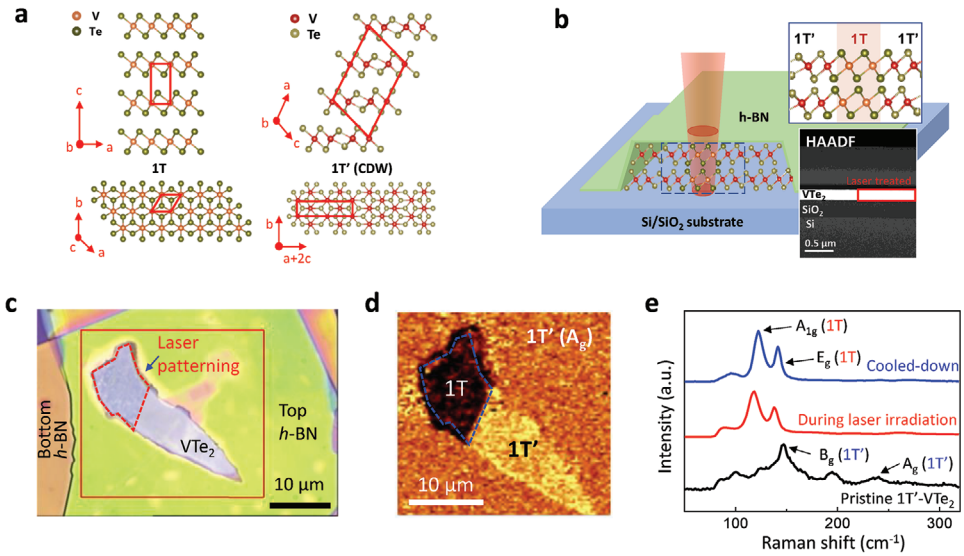

Figure 1. Phase engineering with polymorphic normal and CDW states in VTe_2. a) Lattice structures of 1T- (left) and 1T'-VTe_2 (right). Side and top views are shown with their unit cells (red parallelograms). b) Schematic of a VTe_2 flake encapsulated by an h-BN layer. A laser with 532 nm wavelength was used to locally pattern the phases with various power and exposure time parameters. A HAADF-STEM image is overlaid to show the cross-sectional VTe_2 flake with half irradiated and one-half nonirradiated by the laser. c) An optical image of a VTe_2 flake encapsulated by top and bottom h-BN layers. The red dotted area was irradiated by the laser and false colors are used to indicate the different phase regions. d) A Raman mapping image of the region marked by the red rectangle in "c". e) Point Raman spectra for pristine (black), during laser irradiation (red), and after cooling-down of the laser-irradiated area. An irreversible phase patterning is achieved.

studies with TMDs by using a glove box system, as supported by Raman spectroscopy, and scanning transmission electron microscopy (STEM). In laser irradiation experiments with TMDs, chalcogen atom vacancies, doping, and strain effects have often been found to stabilize certain phases (polymorphs) of the TMDs, where the small energy difference between the polymorphs of the TMDs plays a critical role in the phase transition.

Here, we demonstrate that a polymorphic control of VTe_2 between its CDW (1T') and normal (1T) states can be achieved in a local and robust way by laser irradiation. The polymorphic states, locally patterned with their atomically well-defined lattice structures, remain down to T = 1.5 K, which enables low-temperature investigation of the intrinsic properties of 1T-VTe_2. Raman spectroscopy, TEM, transport measurements, and theoretical calculations were used to confirm the stable, crystalline, and polymorphic states of VTe_2 at low temperatures.

Our transport measurements showed that the two different phases of 1T'- and 1T-VTe_2 not only carry distinct magnetic orderings but also exhibit distinct Kondo behaviors below T = 10 K. These are referred to as polymorphic Kondo effects in this study. Our density functional theory plus dynamical mean-field theory (DFT+DMFT) calculations revealed that the Kondo screening was markedly different in the two polymorphic phases; stronger screening was found in 1T'-VTe_2, consistent with our experiment. Accordingly, we suggest a new way to manipulate spin-lattice coupling via CDW phase patterning, which is promising for designing strongly correlated electronic and magnetic properties in polymorphic TMDs.

2. Results

2.1. Reversible Phase Engineering in VTe_2 by Laser Irradiation

The crystal structures of trigonal 1T (P −3 m 1) and monoclinic 1T' (C 2/m) of VTe_2 are shown in **Figure 1a**. The unit cells of 1T- and 1T'-VTe_2 are marked by red parallelograms and axes in Figure 1a. To distinguish the two phases of VTe_2 in the following discussion, the reference STEM images of VTe_2 were taken along the zone axis [010] at T = 500 K (for the normal state, 1T) and 300 K (for the CDW state, 1T'), as shown in Figure S1a (Supporting Information). The atomic resolution STEM images show two distinct lattice structures for the 1T and 1T' phases. Fast Fourier transform (FFT) patterns of the two images, which are equivalent to the corresponding local diffraction patterns, more clearly distinguish the distinct crystal structures of 1T- and 1T'-VTe_2 (Figure S1a, Supporting Information); a uniform distance between vanadium atoms was observed in the hexagonal 1T-VTe_2, but in the CDW state of 1T'-VTe_2[4] an extended periodicity is formed along the new a-axis and *c*-axis by the double zigzag trimer bonds of vanadium atoms.

To avoid oxidation during laser irradiation, before laser irradiation the VTe_2 flakes were encapsulated by hexagonal boron nitride (h-BN) layers in the glove box, as shown in Figure 1b. The cross-sectional VTe_2 flake on a SiO_2/Si substrate was observed in high-angle annular dark field (HAADF) STEM imaging mode (Figure 1b). The laser-irradiated half of the VTe_2 flake showed the same thickness as the other half of the flake, which was not irradiated by the laser. This result provided no evidence of the oxidation (which generally causes a volume change) of the laser-irradiated VTe_2.

Note that the h-BN overlayer on the VTe_2 was not visible in the HAADF STEM imaging mode due to the relatively low scattering signal. In the absence of oxidation, the laser treatment enables reversible (shown in Figure S1b, Supporting Information) and irreversible phase transitions (shown in Figure 1c–e) between 1T- and 1T'-VTe_2, which can be selectively and locally tuned by laser power and exposure time. Especially when we used the laser power lower than 0.3 mW, after several hundred seconds, VTe_2 exhibits reversible phase transition. The laser irradiation was conducted using a Raman spectroscopy system (Nanobase XperRAM, South Korea), and thus, Raman spectra could be obtained simultaneously in the irradiation process.

During the reversible phase engineering of the normal (1T) and CDW (1T') states of VTe_2, shown in Figure S1b (Supporting Information), the black curve was obtained before the laser irradiation; the Raman active modes for the Ag and Bg peaks of pristine 1T'-VTe_2 are shown in Figure S1b (Supporting Information). The red curve in Figure S1b (Supporting Information) was taken during laser irradiation, where the Raman active modes of 1T-VTe_2 (known as the high-temperature phase of VTe_2) are shown with the E_g and A_{1g} peaks; the peaks are consistent with reported phonon calculations.[4] After the flakes were laser-treated and cooled down, the Raman spectrum came back to that of 1T'-VTe_2, shown in the blue curve in Figure S1b (Supporting Information).

We note that the relatively low temperature of the CDW transition in VTe_2 (i.e., T = 480 K) allows such reversible phase transition without sublimation of atomic elements (mostly tellurium atoms), and does not apply to other TMDs. For example, the CDW transition of $MoTe_2$ occurs at T = 800 K, and laser irradiation only produces an irreversible phase transition.[6] Compared with the case of $MoTe_2$, VTe_2 exhibits relatively low vapor pressure near the critical temperature, preventing the Te sublimation and preserving the stoichiometric ratio so that phase transition in VTe_2 is reversible. Thus, we note that a reversible and local phase transition between the normal and CDW state by laser irradiation is a unique feature of VTe_2. Here, we used bulky VTe_2 samples with thicknesses of 50 nm or larger to investigate phase transition in bulk VTe_2 with the right stoichiometric ratio.

Laser patterning with a higher local laser power (>3 mW) generates an irreversible phase transition, as shown in Figure 1c–e. A VTe_2 flake, encapsulated by h-BN layers, was used for the local, irreversible phase transition in Figure 1c–e. Mapping the laser irradiation with the high laser power creates a normal phase (1T) region, like the optical image of the laser-treated flake shown in Figure 1c. To demonstrate the phase patterning in the normal and CDW states, additional Raman mapping (with a low laser power) of the Ag peak (240 cm^{-1}) of 1T'-VTe_2 is shown in Figure 1d. The red dotted area in Figure 1c indicates the Raman mapping area in Figure 1d. The point Raman spectra in Figure 1e exhibit the remaining 1T region after the laser-treated area is cooled down.

2.2. Atomic-Scale Verification of the Polymorphic CDW Phases in VTe_2

The atomic-scale lattice structures and local crystal symmetries of the laser-patterned and pristine areas were investigated by STEM combined with position-averaged convergent beam electron diffraction (PACBED).[29] A VTe_2 flake with both phase patterned and pristine areas was transferred onto a TEM grid, as shown in **Figure 2a**. The "laser-irradiated" and "pristine" regions in Figure 2a were chosen for STEM and PACBED analyses, which indicated the two areas of the laser patterned (i.e., the normal 1T phase) and the pristine (1T') areas, respectively, could be distinguished. Since the contrast in PACBED is sensitively altered depending on subtle changes in crystal symmetry, polymorphic phases with a similar lattice framework can be reliably distinguished.[30] To identify the crystal structures of the laser-irradiated and pristine regions, we acquired PACBED patterns of the two regions, as shown in Figure 2b. By comparing the experimental PACBED patterns (Figure 2b, left) with the simulated PACBED patterns calculated from the [001]-oriented 1T and [$\bar{1}$01]-oriented 1T' structures (Figure 2b, middle), we confirmed that the two regions were the 1T (P $\bar{3}$ m1) and 1T' (C2/m) phases, respectively. The experimental plane-view atomic structures of the 1T and 1T' phases observed by STEM also show an excellent match with the simulated images obtained from the structures identified by the PACBED results (Figure 2b, right).

The lattice images obtained by STEM along the zone axis of [010] and the corresponding FFT patterns of the two areas also demonstrated that the laser-treated area has a 1T structure, while the pristine area retained a 1T' structure (Figure 2c). The two identified structures were consistent with our reference STEM results shown in Figure S1 (Supporting Information). These results indicate that the phase transition between the two states occurs over the entire region (not only close to the surface) following laser irradiation. We note that this is unique among various TMDs; it has been reported that the laser-driven phase transition occurs mostly near the top surface (e.g., $MoTe_2$).[31] This indicates that induced chalcogen vacancies near the surface area do not have the primary role in the phase transition. Instead, the efficient heat transfer leads to the uniform phase transition in the vertical direction of 1T and 1T' phases of VTe_2.

To confirm the vertical range of irreversible phase engineering with the normal 1T phase, cross-sectional STEM images were taken near the phase boundary and compared with the reference TEM images of the 1T and 1T' phases in Figure S1c (Supporting Information). As shown in the inset of Figure 2a and Figure S1c (Supporting Information), the thickness and the atomic element distribution were not changed by the laser local irradiation, which further supports the absence of oxidation during the laser treatment. This indicates the distinctive mechanism of phase patterning in VTe_2 without chalcogen sublimation, enabling the robust phase transition in the entire region of bulk VTe_2 into the high-temperature phase. By STEM images, we can confirm the generation of phase transition without severe collapse of stoichiometric ratio or oxidation in the laser-irradiated sample for PACBED measurements.

2.3. Transport Measurements of the Polymorphic Kondo Effects in VTe_2

Transport studies, including four-probe measurements, magnetoresistance (MR), and Hall measurements, could be conducted at various temperatures with the stable normal state of the CDW material, 1T-VTe_2. We also note that the intrinsic

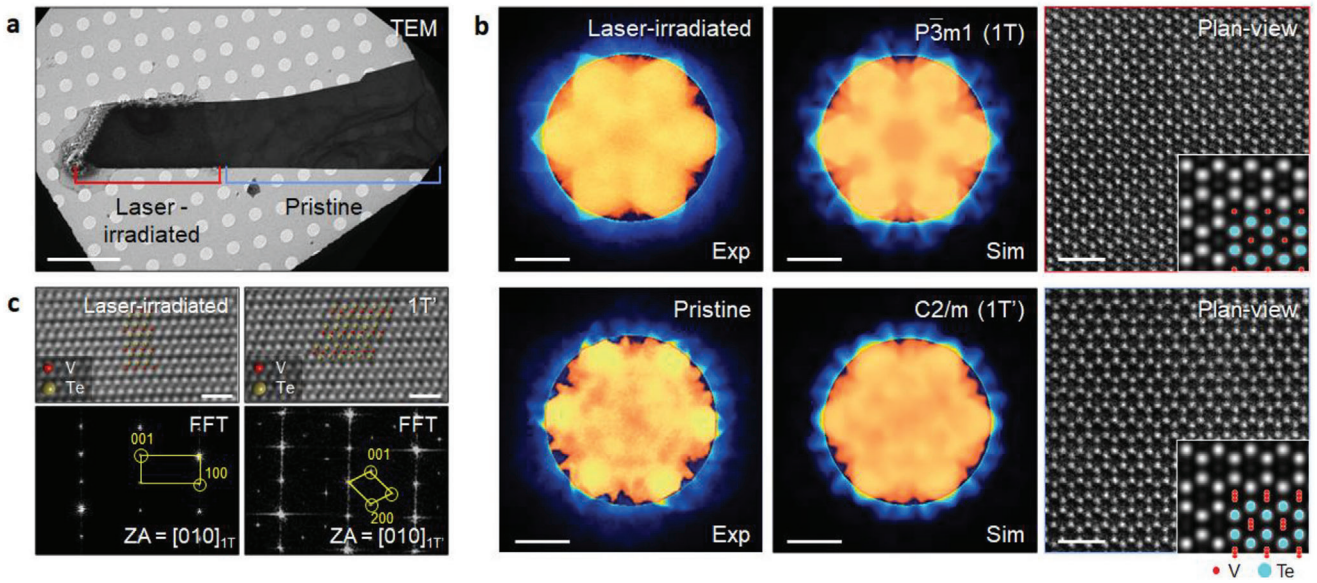

Figure 2. (S)TEM analysis of the phase patterned areas of VTe_2. a) A TEM image of a VTe_2 flake with a partly laser-irradiated area. The flake is put on a grid for STEM. The scale bar is 5 µm. b) (left) Experimental PACBED of the regions denoted "Laser-irradiated" and "Pristine" in "a". (middle) Simulated PACBED patterns. Scale bars are 10 mrad. (right) Plane-view atomic structure of the 1T and 1T' phases compared with the corresponding simulated images. c) Cross-sectional STEM images of the phase patterned (1T) and pristine (1T') areas and their FFT patterns. Unit cells are described by yellow parallelograms. Scale bars are 1 nm.

low-temperature properties of the high-temperature phase (1T-VTe_2) could be investigated and compared with 1T'-VTe_2 in the same device at low temperatures; a 1T'-VTe_2 device was prepared and measured first, and then, a 1T-VTe_2 device could be fabricated by phase patterning the same device.

We fabricated six electrodes, and then a flake of 1T'-VTe_2 was transferred onto the electrodes. To protect the device channel, a thick h-BN layer was used as a passivation layer, as shown in **Figure 3a**. Then, laser irradiation was performed on the entire area of the 1T'-VTe_2 flake. The resulting phase transition was confirmed by Raman spectroscopy; 1T-VTe_2 was observed without the Ag and Bg peaks of 1T'-VTe_2, which is consistent with Figure 1e and Figure S1b (Supporting Information).

In Figure 3b,c, we compare the transport results of 1T- and 1T'-VTe_2. The pristine CDW state of 1T'-VTe_2 exhibits clear Kondo effects, manifested by the negative MR at T = 2 K (the red curve in Figure 3b) and a sudden increase of resistivity below T = 10 K (the red curve in Figure 3c; Figure S5, Supporting Information). We note that former studies on the Kondo screening effect in VTe_2 did not carefully consider the polymorphic aspects of 1T- and 1T'-VTe_2.[24,27]

The comparison results in Figure 3b,c were obtained from the same device; a device with pristine 1T'-VTe_2 was first investigated, and then, the device channel was converted to 1T-VTe_2 by laser-driven, complete, and irreversible phase transition. The normal phase 1T-VTe_2 channel, whose phase was engineered from the pristine CDW state (1T'-VTe_2) in the same device, showed a weaker Kondo screening (see also Figure S2, Supporting Information) or its absence, as demonstrated by the disappearance of the negative MR (blue curve) at T = 2 K in Figure 3b and the monotonic increase in resistivity with temperature (blue curve) in Figure 3c. Hall measurements revealed that the two polymorphic states possessed distinctive carrier densities (Figure 3d).

While negative MR was constantly observed in both vertical and horizontal magnetic fields in the pristine 1T'-VTe_2, we discovered that the absence of Kondo screening or weaker Kondo screening effects appeared in 1T-VTe_2 depending on the carrier density (Figure S2, Supporting Information). 1T-VTe_2 is stable and showed no further phase transition to 1T'-VTe_2 in our transport measurements; for example, the resistivity of 1T-VTe_2 did not abruptly change to its CDW 1T' state at low temperatures, as shown in Figure 3c. The lower resistivity with a lower carrier density of 1T-VTe_2 (shown in Figure 3c,d) indicates 1T-VTe_2 has a higher carrier mobility than pristine 1T'-VTe_2. We note that the higher carrier mobility excludes the possibility of trivial defect formation (e.g., oxidation) by the laser irradiation.

2.4. Theoretical Interpretation of the Polymorphic Kondo Effects in VTe_2

To further elucidate the polymorphic Kondo effects, we compared the magnetic long-range interaction (i.e., exchange interaction, $\hat{H}_{ij} = -J_{ij}\,\hat{s}_i \cdot \hat{s}_j$ with lattice indices i and j) and the Kondo screening strength in the two phases by means of first-principles calculations combined with DMFT.[32–37] While the localized moments are screened by conducting electrons in the original Kondo model, lattice-type Kondo interactions can be around in polymorphic VTe_2 having the localized V-3d moments and the itinerant Te-5p electrons.[38,39] Within the sense of the standard Doniach phase diagram,[32,33] **Figure 4** presents the

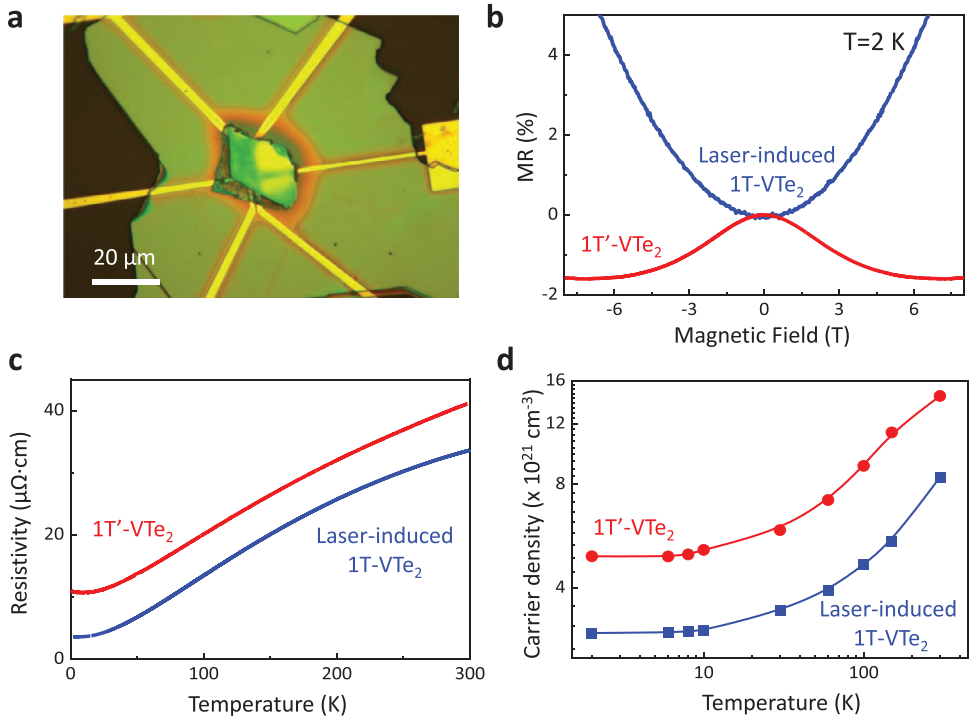

Figure 3. Transport studies of the normal (1T) and CDW (1T') states and polymorphic Kondo effects with VTe_2. a) An optical image of a VTe_2 device. Six electrodes were first made and a VTe_2 flake was then transferred onto the electrodes. Transport measurements were conducted with a 1T-VTe_2 device. After the measurements, laser patterning was done on the whole channel area of the same device, where transport results with 1T'-VTe_2 could be obtained. A thick h-BN layer was deposited on the entire device area to protect the VTe_2 against possible oxidation. b) MR of the normal (1T) and CDW (1T') states of VTe_2 by in-plane magnetic fields. Clear Kondo signature, negative in-plane MR, is observed with 1T'-VTe_2 (red curve). c) Resistivity versus temperature for 1T- and 1T'-VTe_2. No further phase transition was observed by temperature in the two samples. d) Carrier density versus temperature for 1T- and 1T'-VTe_2 by Hall measurements.

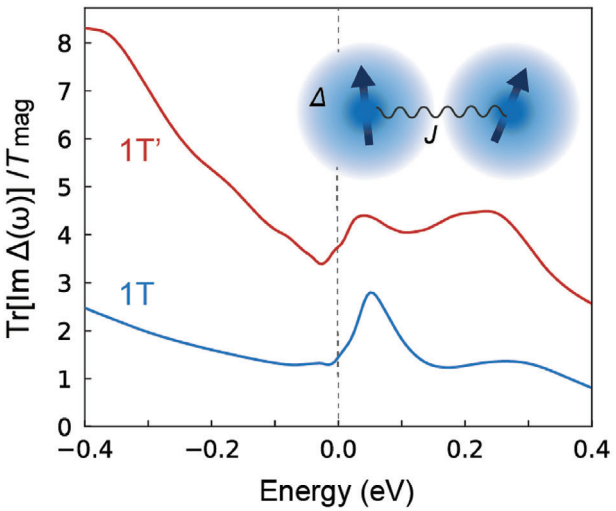

Figure 4. DMFT results of 1T- and 1T'-VTe_2. The calculated hybridization function Tr [Im $\Delta(\omega)$] with respect to the magnetic coupling T_{mag} for the 1T (blue) and 1T' (red) phases of VTe_2. The inset is a schematic of the hybridization Δ by itinerant electrons and magnetic coupling J in VTe_2.

calculated Kondo screening strength (as measured by DMFT hybridization function, Tr [Im $\Delta(\omega)$], around the Fermi level) relative to the local magnetic moment formation (as measured by J_{mag}). In the standard Doniach phase diagram, Figure 4 presents the calculated Kondo screening strength (as measured by DMFT hybridization function, Tr [Im $\Delta(\omega)$], around the Fermi level) relative to the local magnetic moment formation (as measured by J_{mag}). Kondo scattering is clearly greater in the CDW state (1T'-VTe_2; red color) than in the normal state (1T-VTe_2; blue color) over the wide range across the Fermi level. The weaker Kondo effect in 1T-VTe_2 is in good agreement with the absence (or weaker signal) of negative MR and the monotonic resistivity changes in Figure 3b,c.

3. Discussion

Reversible and irreversible local phase transitions for the normal (1T) and CDW (1T') states of VTe_2 were achieved by laser patterning. While the 1T phase has been known to be a high-temperature (normal) phase, our 1T-VTe_2 remained stable down to T = 1.5 K without substrate or strain effects. This unique stability, based on the small energy difference between the phases, allows the intrinsic low-temperature properties, such as magnetic ordering and Kondo screening of the normal state (1T-VTe_2) to be investigated. Accordingly, the polymorphism and effective modulation of the exchange interaction in VTe_2 could be demonstrated as polymorphic Kondo effects. The manipulation of spin-lattice coupling via laser-driven CDW transition enables the design of intrinsic magnetic and correlated physics in TMDs.

Supporting Information

Supporting Information is available from the Wiley Online Library or from the author.

Acknowledgements

This work was supported by the Samsung Research Funding & Incubation Center of Samsung Electronics under project no. SRFC-MA1701-52, the National Research Foundation of Korea (NRF) under Grant No. NRF-2021M3H4A1A03054856 and NRF-2018M3D1A1058793, and the Korea Basic Science Institute (KBSI) National Research Facilities & Equipment Center (NFEC) grant funded by the Korea government (Ministry of Science and ICT) (NO.PG2022004-09). M.J.H was supported by the National Research Foundation of Korea (NRF) grant funded by the Korea government (MSIT) (No. 2021R1A2C1009303 and No. NRF2018M3D1A1058754). S.C. was supported by the Commercialization Promotion Agency for R&D Outcomes (COMPA) funded by the Ministry of Science and ICT (MSIT) (1711196065).

Conflict of Interest

The authors declare no conflict of interest.

Author Contributions

D.W. and D.H.K. contributed equally to this work. H.Y., S.C., and M.J.H. conceived the idea and supervised the project. D.W. and W.C. performed the sample growth and transport measurements. S.-H.Y., Y.-H.K., and Y.-M.K. performed (S)TEM measurements and analyzed the data. D.H.K. and M.J.H. did a theoretical study. All authors contributed to data analysis, result interpretation, and writing the manuscript.

Data Availability Statement

The data that support the findings of this study are available from the corresponding author upon reasonable request.

Keywords

charge density waves, kondo effects, laser irradiation, phase transition, spin-lattice coupling

Received: October 24, 2023
Revised: January 2, 2024
Published online:

[1] V. Vano, M. Amini, S. C. Ganguli, G. Chen, J. L. Lado, S. Kezilebieke, P. Liljeroth, *Nature* **2021**, *599*, 582.
[2] D. Kim, J. Pandey, J. Jeong, W. Cho, S. Lee, S. Cho, H. Yang, *Chem. Rev.* **2023**, *123*, 11230.
[3] D. Costanzo, S. Jo, H. Berger, A. F. Morpurgo, *Nat. Nanotechnol.* **2016**, *11*, 339.
[4] D. Won, D. H. Kiem, H. Cho, D. Kim, Y. Kim, M. Y. Jeong, C. Seo, J. Kim, J.-G. Park, M. J. Han, H. Yang, S. Cho, *Adv. Mater.* **2020**, *32*, 1906578.
[5] L. Ma, C. Ye, Y. Yu, X. F. Lu, X. Niu, S. Kim, D. Feng, D. Tománek, Y.-W. Son, X. H. Chen, Y. Zhang, *Nat. Commun.* **2016**, *7*, 10956.
[6] S. Cho, S. Kim, J. H. Kim, J. Zhao, J. Seok, D. H. Keum, J. Baik, D.-H. Choe, K. J. Chang, K. Suenaga, S. W. Kim, Y. H. Lee, H. Yang, *Science* **2015**, *349*, 625 .
[7] H. Yang, S. W. Kim, M. Chhowalla, Y. H. Lee, *Nat. Phys.* **2017**, *13*, 931.
[8] D. H. Keum, S. Cho, J. H. Kim, D.-H. Choe, H.-J. Sung, M. Kan, H. Kang, J.-Y. Hwang, S. W. Kim, H. Yang, K. J. Chang, Y. H. Lee, *Nat. Phys.* **2015**, *11*, 482 .
[9] D. Kim, E.-C. Shin, Y. Lee, Y. H. Lee, M. Zhao, Y.-H. Kim, H. Yang, *Nat. Commun.* **2022**, *13*, 4516.
[10] S. Kim, S. Song, J. Park, H. S. Yu, S. Cho, D. Kim, J. Baik, D.-H. Choe, K. J. Chang, Y. H. Lee, S. W. Kim, H. Yang, *Nano Lett.* **2017**, *17*, 3363.
[11] Y. Yu, F. Yang, X. F. Lu, Y. J. Yan, Y.-H. Cho, L. Ma, X. Niu, S. Kim, Y.-W. Son, D. Feng, S. Li, S.-W. Cheong, X. H. Chen, Y. Zhang, *Nat. Nanotechnol.* **2015**, *10*, 270.
[12] Y. Qi, P. G. Naumov, M. N. Ali, C. R. Rajamathi, W. Schnelle, O. Barkalov, M. Hanfland, S.-C. Wu, C. Shekhar, Y. Sun, V. Süß, M. Schmidt, U. Schwarz, E. Pippel, P. Werner, R. Hillebrand, T. Förster, E. Kampert, S. Parkin, R. J. Cava, C. Felser, B. Yan, S. A. Medvedev, *Nat. Commun.* **2016**, *7*, 11038.
[13] Y. A. Eshete, E. Hwang, J. Kim, P. L. Nguyen, W. J. Yu, B. S. Kong, M. S. Jang, J. Lee, S. Cho, H. Yang, *Adv. Mater.* **2023**, *35*, 2209089.
[14] R. Kappera, D. Voiry, S. E. Yalcin, B. Branch, G. Gupta, A. D. Mohite, M. Chhowalla, *Nat. Mater.* **2014**, *13*, 1128.
[15] H. Ryu, Y. Lee, J. H. Jeong, Y. Lee, Y. Cheon, K. Watanabe, T. Taniguchi, K. Kim, H. Cheong, C. -H. Lee, G. -H. Lee, *Small* **2023**, *19*, 2205224.
[16] M. Liu, C. Wu, Z. Liu, Z. Wang, D.-X. Yao, D. Zhong, *Nano Res.* **2020**, *13*, 1733.
[17] Y. Wang, J. Ren, J. Li, Y. Wang, H. Peng, P. Yu, W. Duan, S. Zhou, *Phys. Rev. B* **2019**, *100*, 241404.
[18] G. Duvjir, J. -A. Jung, T. T. Ly, N. H. Lam, Y. J. Chang, S. Lee, H. Kim, J. Kim, *APL Mater.* **2022**, *10*, 111102.
[19] P. K. J. Wong, W. Zhang, J. Zhou, F. Bussolotti, X. Yin, L. Zhang, A. T. N'Diaye, S. A. Morton, W. Chen, J. Goh, M. P. Jong, Y. P. Feng, A. T. S. Wee, *ACS Nano* **2019**, *13*, 12894.
[20] T. Ohtani, K. Hayashi, M. Nakahira, H. Nozaki, *Solid State Commun.* **1981**, *40*, 629.
[21] G. Miao, S. Xue, B. Li, Z. Lin, B. Liu, X. Zhu, W. Wang, J. Guo, *Phys. Rev. B* **2020**, *101*, 035407.
[22] K. Sugawara, Y. Nakata, K. Fujii, K. Nakayama, S. Souma, T. Takahashi, T. Sato, *Phys. Rev. B* **2019**, *99*, 241404.
[23] P. M. Coelho, K. Lasek, K. N. Cong, J. Li, W. Niu, W. Liu, I. I. Oleynik, M. Batzill, *J. Phys. Chem. Lett.* **2019**, *10*, 4987.
[24] H. Liu, Y. Xue, J.-A. Shi, R. A. Guzman, P. Zhang, Z. Zhou, Y. He, C. Bian, L. Wu, R. Ma, J. Chen, J. Yan, H. Yang, C.-M. Shen, W. Zhou, L. Bao, H.-J. Gao, *Nano Lett.* **2019**, *19*, 8572.
[25] O. Concepción, L. Mulder, D. H. Wielens, A. Brinkman, *Solids* **2022**, *3*, 500.
[26] Z.-L. Zhu, Z.-L. Liu, X. Wu, X.-Y. Li, J.-A. Shi, C. Liu, G.-J. Qian, Q. Zheng, L. Huang, X. Lin, J.-O. Wang, H. Chen, W. Zhou, J.-T. Sun, Y.-L. Wang, H.-J. Gao, *Chin. Phys. B* **2022**, *31*, 077101.
[27] X. Ding, J. Xing, G. Li, L. Balicas, K. Gofryk, H.-H. Wen, *Phys. Rev. B* **2021**, *103*, 125115.
[28] I. Kar, S. Ghosh, S. Gupta, S. Chakraborty, S. Thirupathaiah, Observation of Kondo effect in transition metal dichalcogenides VX 2 (X = Se & Te) due to low-temperature weak ferromagnetism, **2023**, https://doi.org/10.21203/rs.3.rs-2525938/v1.
[29] S. J. Pennycook, C. Li, M. Li, C. Tang, E. Okunishi, M. Varela, Y. -M. Kim, J. H. Jang, *J Anal Sci Technol.* **2018**, *9*, 11.
[30] Y.-H. Kim, S.-H. Yang, M. Jeong, M.-H. Jung, D. Yang, H. Lee, T. Moon, J. Heo, H. Y. Jeong, E. Lee, Y.-M. Kim, *Small* **2022**, *18*, 2107620.
[31] S. Kang, D. Won, H. Yang, C.-H. Lin, C.-S. Ku, C.-Y. Chiang, S. Kim, S. Cho, *Appl. Surf. Sci.* **2021**, *563*, 150282.
[32] S. Doniach, *Physica B + C* **1977**, *91*, 231.
[33] M. J. Han, X. Wan, S. Y. Savrasov, *Phys. Rev. B* **2008**, *78*, 060401.

[34] Y.-F Yang, Z. Fisk, H.-O. Lee, J. Thompson, *Nature* **2008**, *454*, 611.
[35] M. Matsumoto, M. J. Han, J. Otsuki, S. Y. Savrasov, *Phys. Rev. Lett.* **2009**, *103*, 096403.
[36] Q. Si, S. Rabello, K. Ingersent, J. L. Smith, *Nature* **2001**, *413*, 804.
[37] H. v. Löhneysen, A. Rosch, M. Vojta, P. Wölfle, *Rev. Mod. Phys.* **2007**, *79*, 1015.
[38] A. C. Hewson, *The Kondo Problem to Heavy Fermions*, Cambridge University Press, Cambridge, UK **1997**.
[39] A. Georges, G. Kotliar, W. Krauth, M. J. Rozenberg, *Rev. Mod. Phys.* **1996**, *68*, 13.